Evolutionary constraints from infrared source counts

Chris P. Pearson[★][†]

Institute of Space and Astronautical Science, Yoshinodai 3-1-1, Sagamihara, Kanagawa 229 8510, Japan

ABSTRACT

The backward evolution approach to modelling galaxy source counts is re-visited in the wake of the numerous results and revelations from the *Infrared Space Observatory* (*ISO*), the Submillimetre Common User Bolometer Array (SCUBA) and the detections and measurements of the cosmic extragalactic background light. Using the framework of the Pearson & Rowan-Robinson galaxy evolution model, the observed source counts and background measurements are used to constrain the evolution in the galaxy population. It is found that a strong evolution in both density and luminosity of the high-luminosity tail of the infrared (IR) luminosity function, interpreted as the ultraluminous galaxies discovered first by *IRAS* and later elevated in status by SCUBA and *ISO*, can account for the source counts from 15 μm (where it matches the undulations in the integral counts and the hump in the differential counts extremely well) to the submillimetre region, as well as explain the peak in the cosmic infrared background at $\sim 140\,\mu$m. The submillimetre counts are interpreted as the superposition of two separate populations comprising ultraluminous infrared galaxies (ULIGs) at the brighter submillimetre fluxes and starburst galaxies at fluxes fainter than ~ 2 mJy. In this scenario the high-redshift ULIGs are tenuously interpreted as the progenitors of today's giant elliptical (gE) galaxies.

All the source count models can be accessed via the world wide web at the URL http://www.ir.isas.ac.jp/~cpp/counts/

Key words: galaxies: evolution – infrared: galaxies.

1 INTRODUCTION

The formation epoch of galaxies has long been the Holy Grail of cosmology. Traditionally, one of the most popular and successful ways of glimpsing this epoch has been the analysis of extragalactic source counts or, more commonly, galaxy number counts. Although originally intended to be a means of determining the geometry of the Universe, this tool has shown to be much more viable and useful in the study of the evolutionary and star formation history of galaxies (Kirshner et al. 1981; Ellis 1987). In particular, the large dust content of galaxies discovered by *IRAS* and the strong *K*-corrections have made the infrared (IR) and, more recently, the submillimetre extremely important wavebands for the study of galaxy evolution and cosmic star formation. By modelling the counts of galaxies it has become possible to analyse the evolution of the galaxy population out to redshifts of unity and higher. Coupled with the advent of new observational data, galaxy

number counts are poised to discriminate between rivalling evolutionary theories.

Recently, it has become the vogue to tackle the problem of number distribution of galaxies in the Universe using one of the two methods. The first [often called the backward evolution approach (Lonsdale 1996)], takes the observed, present-day ($z = 0$) luminosity function and evolves it in luminosity and/or density back out to higher redshifts assuming some parametrization of the evolution (Beichman & Helou 1991; Blain & Longair 1993; Pearson & Rowan-Robinson 1996, hereafter cppRR; Xu et al. 1998; Takeuchi et al. 1999). This method has the advantage of it being both direct and relatively simple to implement, with few free parameters and assumptions about the Universe at earlier times. The disadvantage in the past was that the information on which the assumptions about evolution were made often came from *IRAS* data which extended out only to relatively low redshifts ≈ 0.02–0.2. In the alternative method, known as the forward evolution approach, the evolution is computed assuming some initial conditions of the physical processes of chemical evolution and photometric evolution of the stellar populations that heat the dust (Franceschini et al. 1994). The so-called semi-analytical approach combines these assumptions on the chemical/photometric evolution of galaxies, with models considering the dissipative and

[★]E-mail: c.pearson@ic.ac.uk
[†]Present address: Astrophysics Group, Imperial College of Science, Technology and Medicine, Blackett Laboratory, Prince Consort Road, London SW7 2BW.

non-dissipative processes affecting galaxy formation within dark-matter haloes (Cole et al. 1994; Baugh, Cole & Frenk 1996) and has provided a reasonable fit to the source counts in the infrared (Guiderdoni et al. 1998). The forward evolution approach has the advantage of being based on perhaps a more fundamental set of assumptions. However, the obvious disadvantage is the larger number of free/unknown parameters assumed in these models.

Furthermore, with the recent advent of large, deep surveys by SCUBA (Holland et al. 1999, e.g. Smail, Ivison & Blain 1997; Barger et al. 1998; Hughes et al. 1998; Barger et al. 1999a; Blain et al. 1999a), and *ISO* (Kessler et al. 1996, e.g. Bogun et al. 1996; Serjeant et al. 1997; Taniguchi et al. 1997; Elbaz et al. 1998; Kawara et al. 1998; Stickel et al. 1998; Altieri et al. 1999; Flores et al. 1999a,b; Lindern-Vørnle et al. 2000; Oliver et al. 2000a,b), including constraints on the source counts to fainter levels and the IR background (Lagache et al. 1999, 2000; Matsuhara et al. 2000; Matsumoto et al. 2000) and detections by the *COBE* Far Infrared Absolute Spectrometer (FIRAS)/Diffuse Infrared Background Experiment (DIRBE) instruments at 140 and 240 µm (Puget et al. 1996; Fixsen et al. 1998; Hauser et al. 1998), the tools are now available to constrain the backward evolution methodology to significantly higher redshifts. In the light of these recent advances in the millimetre-IR region the backward evolution method is re-visited.

The aim of this paper is not to produce a definitive evolutionary model to fit all observed counts while satisfying various preferences on the various dominant populations [starburst, active galactic nuclei (AGN), LIG ($L_{IR} > 10^{11}$ L$_\odot$), ultraluminous galaxies (ULIGs $L_{IR} > 10^{12}$ L$_\odot$), and hyperluminous galaxies ($L_{IR} > 10^{13}$ L$_\odot$)]. Rather, I seek to investigate the various avenues of evolution that can viably fit the galaxy source counts from the mid-IR to the submillimetre without violating the constraints set by the IR background and cosmic microwave background (CMB) measurements. The paper is structured as follows: in Section 2 the galaxy count and world model parameters are outlined. Section 3 reviews current evolutionary models, constraints and analyses simple density and luminosity evolution scenarios. Section 4 formulates a new evolutionary source count model and applies it to the observed source counts and background measurements from the mid-IR to the submillimetre wavelengths. The possible interpretations and conclusions are reported in Sections 5 and 6, respectively.

2 MODEL PARAMETERS

In general, for observations at frequency $\nu = c/\lambda$, the total number of sources per steradian observable down to a flux sensitivity S is given by;

$$N(S_\nu) = \int_0^\infty \int_0^{z(L,S)} \phi[L/f(z)] \frac{dV(z)}{dz} g(z) \, d\log L \, dz, \qquad (1)$$

where

$$\frac{dV(z)}{dz} = \frac{4\pi D^2}{H_0(1+z)^2(1+\Omega_o z)^{1/2}}, \qquad (2)$$

and $\phi = d\Phi/d\log L$ is the zero redshift differential luminosity function per decade in luminosity L, parametrizing the number density of extragalactic sources as a function of luminosity at a frequency ν. dV/dz is the general form of the differential volume element with redshift, z, and is dependent on the luminosity distance, D, and the assumed cosmological world model. $f(z)$ and

$g(z)$ are the luminosity and density evolutionary parameters, respectively. The limiting redshift $z(L, S)$, is determined by the flux S, below which a source of luminosity L, becomes too weak to be included in the sample of galaxies observed, where

$$S(\nu_o) = \frac{L_{\nu_o}}{4\pi D^2} \frac{\nu_e L_{\nu_e}}{\nu_o L_{\nu_o}} f(z), \qquad (3)$$

$$D(z) = \frac{2c}{H_0 \Omega_o^2} \{\Omega_o z + (\Omega_o - 2)[(1 + \Omega_o z)^{1/2} - 1]\}. \qquad (4)$$

Here $\nu_e L_{\nu_e}/\nu_o L_{\nu_o}$ is effectively the ratio of the emission luminosity (luminosity at ν_e) to the observed luminosity (i.e. the K-correction). Even assuming a single luminosity function and an evolutionary history for all extragalactic sources can, in fact, come impressively close to matching the true numbers and distribution of sources over a wide range of wavelengths as observed in the Universe (e.g. Takeuchi et al. 1999, 2001).

cppRR provided an impressively solid framework from which the source counts from radio frequencies, submillimetre, IR, optical, UV wavelengths to X-ray energies were modelled. The original IR models of cppRR consisted of a four-component parametrization of the extragalactic population based on the IR colours of *IRAS* galaxies (Rowan-Robinson & Crawford 1989). The model incorporated a normal galaxy (IR cirrus dominated) component defined by cool 100/60 µm colours, a starburst component defined by warm 100/60 µm colours extending to an ultra/hyperluminous component at higher IR luminosities and an AGN Seyfert/quasi-stellar object (QSO) 3–30 µm dust torus component defined by low 60/25 µm colours. The basic framework of this model has been maintained in this further analysis.

The original template spectral energy distributions (SEDs) of Rowan-Robinson (1992) and Rowan-Robinson & Efstathiou (1993) for the cool normal, warm starburst and ultraluminous galaxies are replaced by the new radiative transfer models of Efstathiou & Siebenmorgen (in preparation) and Efstathiou, Rowan-Robinson & Siebenmorgen (2000a), respectively. The new starburst galaxy models are calculated by considering the evolution of an ensemble of optically thick giant molecular clouds, illuminated by embedded massive stars. The starburst models are defined by the parameters t, the age of the starburst in Myr, τ, the initial optical depth (in V) of the molecular clouds and χ, the ratio of the radiation field to the local solar neighbourhood. The starburst SED can be considered akin to M82, while the ULIG SED represents an Arp 220 type galaxy. The introduction of this Arp 220 type SED replaces the more extreme hyperluminous galaxy *IRAS* F10214 (Rowan-Robinson et al. 1991a, 1993) which was used in the earlier models of cppRR. F10214 does not have a typical ULIG SED and such a hyperluminous galaxy population may represent an even more extreme extension of the starburst phenomenon than the ULIGs, only 39 being identified (Rowan-Robinson 2000) so far. Efstathiou et al. (2000a) demonstrated that exponentially decaying $10^7 \sim 10^8$ yr old starbursts are capable of reproducing both the *IRAS* colours of galaxies, and also provide good fits to the data for the stereotypical starburst galaxy M82 and to the starburst galaxy NGC 6090 recently observed by *ISO* (Acosta-Pulido et al. 1996).

Of particular importance to the models in the mid-infrared region is the inclusion of the unidentified infrared bands (UIB), popularly supposed to be band emission from polycyclic aromatic hydrocarbons (PAHs, Puget & Leger 1989), into the model SEDs. These features are prominent from 3–12 µm in most galaxies (Boulade 1996, Lu et al. 1996, Vigroux et al. 1996) having
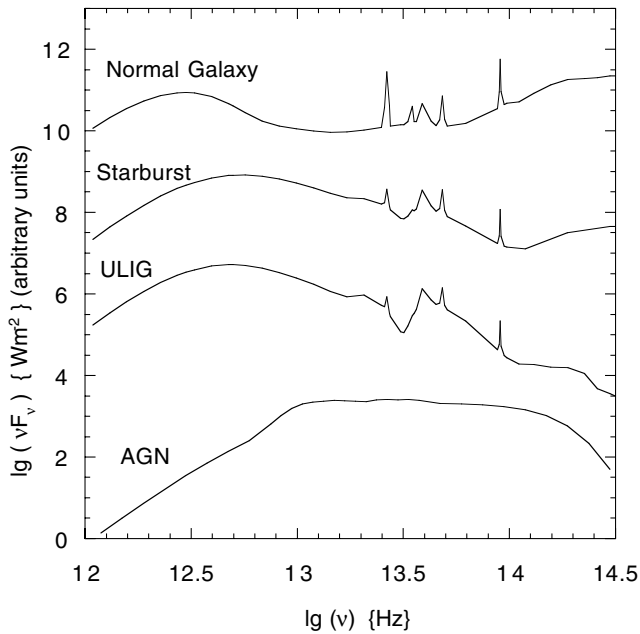
Figure 1. Model SEDs used for the source count models.

Table 1. Luminosity function parameters.

Component	α	σ	β	$\log(L^*/L_\odot)$	C
Cool 60 µm	1.15	0.463	–	9.62	2.000×10^{-3}
Warm 60 µm	1.27	0.626	–	9.99	3.250×10^{-4}
ULIG 60 µm	–	0.1	–	11.6	4.185×10^{-6}
Seyfert 1 12 µm	1	–	2.1	9.552	2.0969×10^{-4}
Seyfert 2 12 µm	1	–	2.5	9.952	8.0251×10^{-5}

parametrizations of *IRAS* galaxies (Soifer et al. 1987a). In this parametrization the normal and starburst galaxies extend in the 60-µm luminosity from $\log L_{60\,\mu m} = 8$–$11.5\,L_\odot$ while the ULIG population forms the high-end tail of the starburst luminosity function from $\log L_{60\,\mu m} = 11.5$–$14\,L_\odot$. The AGN are represented by the 12-µm luminosity function of Lawrence et al. (1986) defined from $\log L_{12\,\mu m} = 8$–$14\,L_\odot$ with parameters corresponding to the 12-µm sample of Rush, Malkan & Spinoglio (1993) for Seyfert 1 and Seyfert 2 galaxies. The parameters for the different components given in Table 1 correspond to those in the equations below for the 60-µm galaxy and 12-µm AGN luminosity functions, respectively;

$$\phi(L_{60}) = \frac{d\Phi}{dL} = C\left(\frac{L}{L^*}\right)^{1-\alpha} \exp\left[-\frac{1}{2\sigma^2}\log^2\left(1 + \frac{L}{L^*}\right)\right], \qquad (5)$$

$$\phi(L_{12}) = \frac{d\Phi}{dL} = CL^{1-\alpha}\left(1 + \frac{L}{L^*\beta}\right)^{-\beta}, \qquad (6)$$

To shift the luminosity function from the wavelength at which it is defined, λ_{LF}, to the observational wavelength, λ_{obs}, the ratio of $L(\lambda_{obs})/L(\lambda_{LF})$ is obtained via the model template spectra.

The model assumes $\Omega = 0.1$ and $H_0 = 50\,\mathrm{km\,s^{-1}\,Mpc^{-1}}$. Alternative cosmologies are not examined in this work so as to ensure that a clear distinction between the evolution scenarios can be made. The maximum redshift assumed for the models is $z = 7$, although assuming a higher redshift of 10 makes little difference to the results presented here.

3 EVOLUTION

3.1 Observational evolutionary evidence

The original cppRR model assumed a simple power-law luminosity evolution $L(z) = L(z = 0)(1 + z)^{3.1}$ for the starburst, ultraluminous and AGN components and was found to fit the *IRAS* data extremely well (Oliver, Rowan-Robinson & Saunders 1992). This evolution was motivated by similar evolutionary models at radio and X-ray wavelengths (Boyle, Shanks & Peterson 1988; Benn et al. 1993; Condon 1994). Recently, similar evolution has also been observed in optically selected starburst galaxies (Lilly et al. 1996) and in the submillimeter emission from radio-loud galaxies observed at 850 µm by SCUBA (Archibald et al. 2001). Although this simple form of evolution still provides a satisfactory fit to source counts down to faint sensitivities [1 mJy at 15 µm, Serjeant et al. (2000), ~0.3 Jy & ~0.1 Jy at 170 and 90 µm, respectively], using this evolution the bumps and dips observed in the *ISO* 15-µm counts below 1 mJy cannot be reproduced and moreover the predicted counts at far-IR wavelengths fall below the observed values completely (e.g. 170 µm FIRBACK; Puget et al. 1999, Lockman Hole; Kawara et al. 1998). Moreover, the extremely high counts reported by the SCUBA instrument at submillimetre wavelengths, at fluxes brighter than ~2 mJy, cannot

equivalent widths of as much as 10 µm, comparable to those of the *ISO*CAM MIR filter bandpasses [3.5 and 6 µm for the LW2 (5–8.5 µm) filter and LW3 (12–18 µm) filter, respectively]. These UIBs are expected to significantly distort the mid-IR source counts compared to those constructed purely on the basis of *IRAS* SED data (Xu et al. 1998; Pearson et al. 2001). A further significant and necessary improvement over the original cppRR model is the introduction of the full range of PAH features (Siebenmorgen & Krugel 1992), which were not considered in the earlier model predictions. Fig. 1 shows the new model SEDs. The shape and form of the PAH features assumed in different models can vary significantly (e.g. see Xu et al. 1998, Dole et al. 2000). However, although the PAH features may seem overly strong or sharply defined, as long as the energy contained within the feature peaks is consistent with observation and the SEDs are correctly smoothed and convolved with the filter response function, the general profile of the individual features is not critical as galaxies will naturally have a range of feature profiles in their SEDs.

Note that recently Dunne et al. (2000a) have shown from the SCUBA data on local galaxies that there is a correlation between the far-IR submillimetre SED and the 60-µm luminosity function. This effect is not treated in the model SEDs and will be the subject of a later investigation.

For the AGN SED the original SED of Rowan-Robinson (1995) is retained. The MIR SED of AGN is relatively featureless compared to that of starburst galaxies, exhibiting none of the broad-band UIB features present in the spectrum of the latter (Lutz et al. 1997). The AGN central engine (black hole) would be expected to produce an extreme environment destroying or changing the smaller dust grains and their composition.

The model components are distinguished on the basis of their SEDs and number–luminosity distributions (i.e. luminosity function). The cool normal galaxies, warm starbursts and ULIG galaxies are well described locally by the *IRAS* 60-µm luminosity function (Saunders et al. 1990), which is a log Gaussian function producing a slightly broader distribution than a traditional Schecter function, and preferable to the slightly less physical power law

be reproduced in any way by the cppRR luminosity evolution model, although it should be noted that the predictions are tantalizingly close to the observed counts at fluxes fainter than $S_{850\,\mu m} < 2\,\text{mJy}$. Furthermore, although the faintest source counts from the 60-μm *IRAS* Very Faint Source Survey (VFSS, ~120 mJy; Gregorich et al. 1995; Oliver et al. 1995; Bertin, Dennefeld & Moshir 1997) could be well explained by the cppRR pure evolution model at these relatively bright fluxes the evolutionary constraints are extremely tenuous with many different scenarios being allowed [the *IRAS* samples not probing to significantly large redshifts QDOT sample $z_{\text{median}} = 0.03$ (Rowan-Robinson et al. 1991b), VFSS analysis $z < 0.3$]. At redshifts higher than ~0.25, the evolution is not well constrained.

Recently, several authors have attempted to combat these shortcomings by incorporating stronger or more drastic evolution scenarios into the source count framework. Rowan-Robinson (2000) included evolution explicitly into the IR 60-μm luminosity function, reproducing many of the observables if a low-density cosmology was assumed ($\Omega_o = 0.3$). For higher values of the density parameter it was concluded that a new, strongly evolving population would have to be invoked (e.g. Franceschini et al. 1998). Takeuchi et al. (2001) treated a global luminosity evolution scenario in a step-wise, non-parametric form, concluding that strong evolution to $z \sim 1$ was necessary to fit the *ISO* source counts at 15 and 170 μm along with the far-IR background. An advantage of the formulation of cppRR was that the 60-μm luminosity function was treated as a superposition of galaxy populations providing the added flexibility of specific evolution with extragalactic class. However, these evolution scenarios must be reviewed if we hope to fit the SCUBA counts at 850 μm and *ISO* faint counts at 15 and 170 μm.

From a statistical analysis of the 60-μm *IRAS* VFSS, Bertin et al. (1997) concluded that the most luminous *IRAS* galaxies should be $\approx 5 \sim 7$ times more numerous at $z \approx 0.3$ than at the present epoch, with IR luminosities of the order of $L_{60} \sim 2 \times 10^{12}$ and optical magnitudes between $20 < B_J < 21$ with red colours (B_J–$R_F \approx 1.6$) making them potential ULIG candidates (Clements et al. 1996). Kim & Saunders (1998) compiled a complete flux limited sample of ULIGs from the *IRAS* Faint Source Catalogue (FSC) with a flux $f_{60} > 1\,\text{Jy}$ to a maximum redshift of $z = 0.268$ and mean redshift of $\langle z \rangle \sim 0.15$. Although locally ($z < 0.1$) ULIGs have a space density approximately similar to optically selected QSOs, the analysis of the *IRAS* FSC hinted at much stronger evolution at higher redshifts to $z \approx 1$, thus outnumbering the QSOs by a factor of 2. Based on the premise that the ULIG population may follow a similar evolutionary track to QSOs (Hassinger 1998; Kim & Saunders 1998) modelled the ULIG population with density evolution of the form $(1 + z)^g$, with $g \approx 7.6 \pm 3.2$. Similar strong density evolution (equivalent to $g \approx 10$ at $z \sim 1$) has also been proposed to fit the deep 15-μm *ISO* source counts (Dole et al. 2000). The vast majority of ULIGs appear to be in the latter stages of merging (98 per cent in the sample of Borne et al. 1999; see also Arribas, Colina & Borne 2000; Borne et al. 2000; Colina et al. 2000) with double nuclei, overlapping discs and tidal features clearly present in many images (Melnick & Mirabel 1990; Clements et al. 1996; Sanders et al. 1998). The large amounts of dust, present in the central regions of these galaxies, provides an ideal environment for circumnuclear starburst and/or AGN, adding to the growing evidence that ULIGs could be the progenitors of todays giant elliptical (gE) galaxies, formed by merger induced collapse of the galaxy core, formation of globular clusters and galactic superwinds resulting in a dust-free core and corresponding
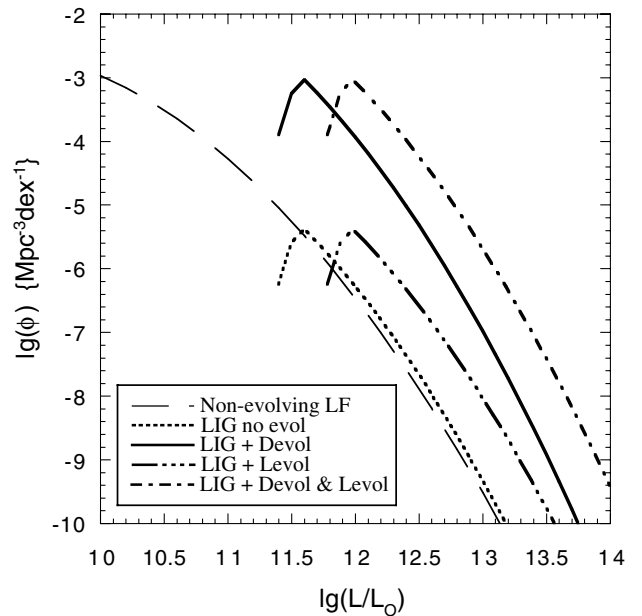

Figure 2. Evolution of the high-luminosity tail of the 60-μm differential luminosity function. The zero redshift (no evolution) 60-μm luminosity function and high-luminosity tail are shown in comparison with an evolved $L^* = 10^{11.6}\,L_\odot$ LIG luminosity function tail at $z = 1$, shown for mild pure luminosity evolution, equivalent to $(1 + z)^{0.5}$, strong pure density evolution, equivalent to $\sim(1 + z)^8$, and a combination of both. Luminosity evolution corresponds to a horizontal displacement in luminosity, whereas density evolution corresponds to a vertical displacement in number density.

enrichment of the intergalactic medium (Kormendy & Sanders 1992; Surace et al. 1998). However, in the local Universe $z \lesssim 0.08$ and the space density of ULIGs is approximately 0.001 per square degree or $\approx 1.1 \times 10^{-7}\,\text{Mpc}^{-3}$ (Saunders et al. 1990), a factor of as much as ≈ 1500 lower than early-type galaxies (Trentham 2000). Thus if ULIGs are to be present in sufficient numbers to account for today's gE galaxy population, then their space density must increase drastically with look-back time (a factor of $1500 \sim 10^{-4}\,\text{Mpc}^{-3}$).

3.2 Evolution of the high-luminosity tail of the IR luminosity function

Under this motivation, extreme number evolution of the ULIG population is considered, i.e. the high-luminosity tail of the 60-μm luminosity function. Fig. 2 shows the effect of such evolution on the 60-μm differential luminosity function. Evolution in the number of galaxies with redshift (density evolution) produces a vertical shift in the luminosity function plane. Evolution in the luminosity of galaxies (luminosity evolution) produces a horizontal shift in the luminosity function plane. In reality a combination of the two scenarios may well be realized. In the figure, only evolution in the high-luminosity tail of the luminosity function is shown. Here I have defined a population of LIG/ULIG with $\log L^* \approx 11.6\,L_\odot$, i.e. corresponding to a far-IR luminosity (50–100 μm) of $\sim 11.8\,L_\odot$ such that the total IR luminosity (1–1000 μm) $\sim 12\,L_\odot$ (Helou, Soifer & Rowan-Robinson 1984). The definition of L^* is given in equations (5) and (6) which define the luminosity functions used in these models. Although the luminosity functions are not classical Schecter functions, the definition of L^* is almost identical. Changing the value of L^* to higher luminosities shifts the luminous infrared population down
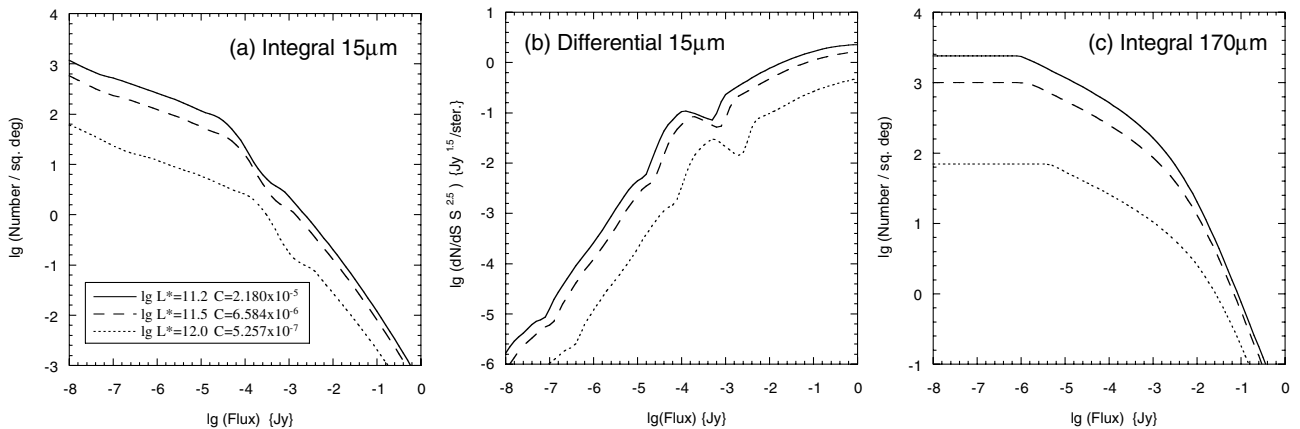
Figure 3. (a) Integral source counts of luminous/ultraluminous IR galaxies at 15 μm, (b) differential counts at 15 μm and (c) integral counts at 170 μm, assuming values of log L^* = 11.2, 11.5, 12 $L_\odot$. The values of C quoted are the corresponding normalizations of the luminosity function given in equation (5) and Table 1. The shift with increasing log L^* to the lower right in the log N/log S plane reflects the higher brightness but lower number density (normalization) of the sources.

and to the right (towards a lower normalization) in the luminosity function plane, and has a similar effect on the corresponding calculated source counts as shown in Fig. 3, where a brighter L^* results in detections at brighter sensitivity limits but at a lower number density (i.e. more powerful but scarcer sources). It should be kept in mind that the main aim of this work is to try to highlight the constraints, by means of simple evolutionary scenarios, on the evolution of the high-end tail of the 60-μm IR luminosity function. [Luminosity functions in other wavebands are also available, e.g. recently the submillimetre luminosity function has been calculated by Dunne et al. (2000a) using the SCUBA Local Universe Galaxy Survey, SLUGS].

As a starting point, I compare the pre-*ISO* view of galaxy evolution with the galaxy source counts observed at 15, 60, 170 and 850 μm by *ISO*, *IRAS*, *ISO* and SCUBA, respectively. Three scenarios are presented for the evolution of the ULIG component, (i) no evolution, (ii) luminosity evolution of the form $f(z) = (1 + z)^{3.1}$ (cppRR model) and (iii) density evolution of the form $g(z) = (1 + z)^7$ (e.g. Oliver et al. 1995). The evolution is continued out to a redshift of 2.5 where it is assumed to level off and eventually decline towards higher redshift. Fig. 4 shows the individually evolving ULIG components plus the total source counts corresponding to each scenario. The total source counts include the ULIG component and the normal, starburst, and AGN components [evolving as $L(z) = f(z)L(0)$ as per the cppRR model framework]. From this simple representation of the evolution we can already ascertain important boundary conditions on the evolution of the ULIG component. At the brightest fluxes all models agree on the same normalization, as they should, considering that at these fluxes the counts do not probe deeply enough to discriminate between the different evolution scenarios. Both the luminosity and the density evolution scenarios are monotonically increasing in power with redshift, so we may interpret a deficit with respect to the observed counts as a lack of evolutionary amplitude at lower redshifts, while an excess with respect to the observed counts may be interpreted as an indication of too much evolution at higher redshifts.

At 15 μm, the integral counts appear to be well fitted by all scenarios with the only discrepancy between the density and luminosity evolution models appearing at the faintest flux levels (remembering that evolution is also present in the other more established components of the cppRR model). Serjeant et al. (2000) found that the 15-μm integral counts could indeed be well

fitted by a variety of evolving models (cppRR, Franceschini et al. 1994; Guideroni et al. 1997; Xu et al. 1998). However, examining the 15-μm differential counts provides a more discriminating picture. The differential counts effectively measure the slope of the integral counts and are hence more sensitive to subtle changes that may not be prominent in the integral counts at first sight. Here again we see a discrepancy between the two evolution scenarios with the density evolution model producing slightly higher differential counts (i.e. steeper integral counts) at the faintest fluxes (perhaps hinting at being marginally inconsistent with the observed counts as a result of too much power at higher redshifts?). However, what is more striking is that neither the classical density nor the luminosity evolution models can reproduce the subtle changes of slope in the 15-μm counts, which are not easily apparent from the integral source counts alone. It is apparent from the differential counts that the counts steepen drastically from ~3–0.4 mJy [log(dN/dS) = α log S, $\alpha \approx -3$] above Euclidean expectations, turn over at ~0.4 mJy and rapidly flatten at fainter fluxes. The analysis by Serjeant et al. (2000) concluded that models incorporating pure luminosity evolution provided a better fit than the density evolving models, although they assumed a lower value for the density evolution. Moreover, their observations did not extend down in detail below 10 mJy in the differential counts.

At 60 μm the *IRAS* data does not really extend to deep enough fluxes to gain meaningful insight from the models, with both the luminosity and density evolution scenarios fitting both the integral and differential counts, although the faintest differential counts would imply stronger evolution than that currently assumed.

However, at 170 μm none of the models can account for the observed source counts at fainter fluxes (although the brightest points are fitted by all models). At 170 μm we could envision a general increase in the magnitude of the evolution as we generally fit the observed counts (i.e. increasing the density evolution power-law index g). However, in the case of density evolution, fitting the FIRBACK counts (Puget et al. 1999) would result in violating the limits set by the fluctuation analysis in the Lockman Hole of Matsuhara et al. (2000), if the trend of a flattening in the source counts is continued below fluxes of 70 mJy. This again points to some constraint on the magnitude of the allowed density evolution if the evolution is allowed to increase monotonically to higher redshifts. If density evolution is to account for the 170-μm counts, without simultaneously violating the fluctuation analysis limits, then it must take place at a relatively low redshift ($z \sim 1$).
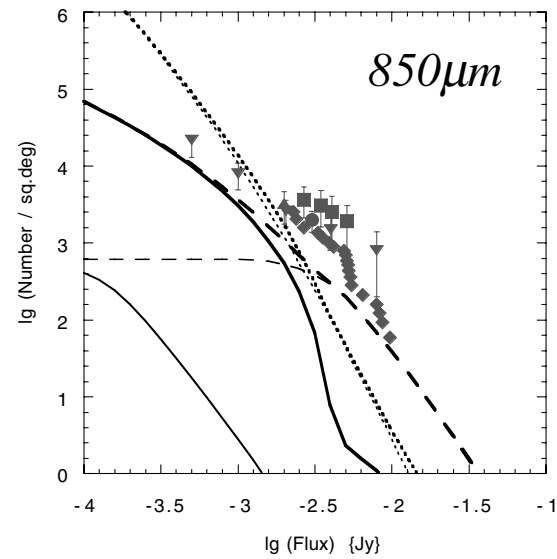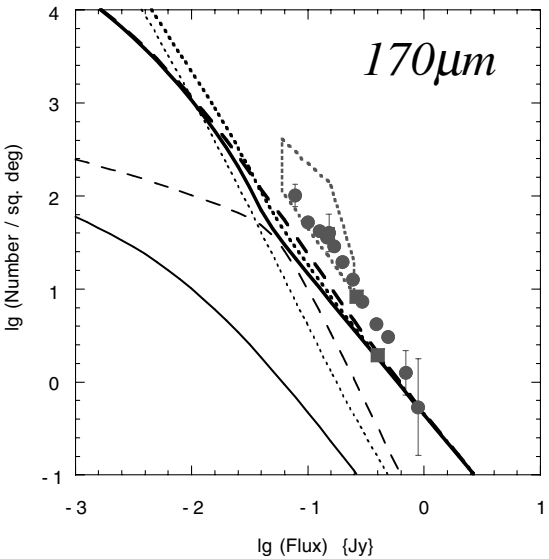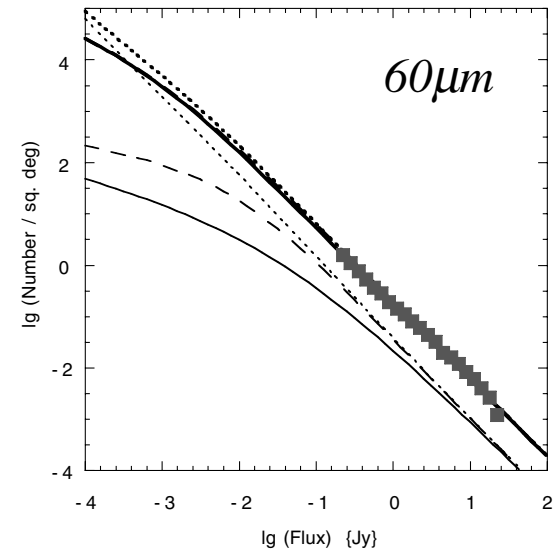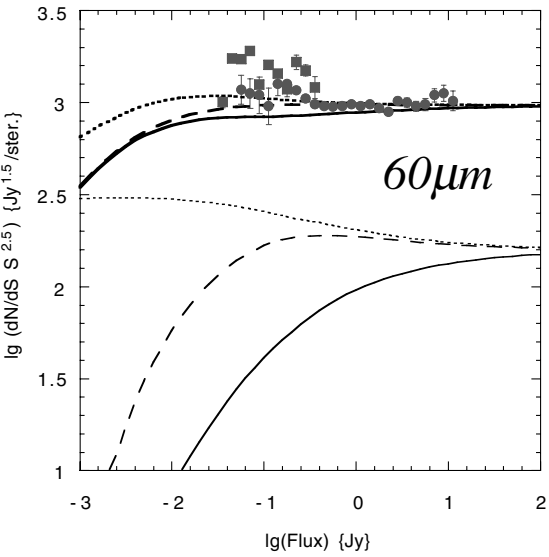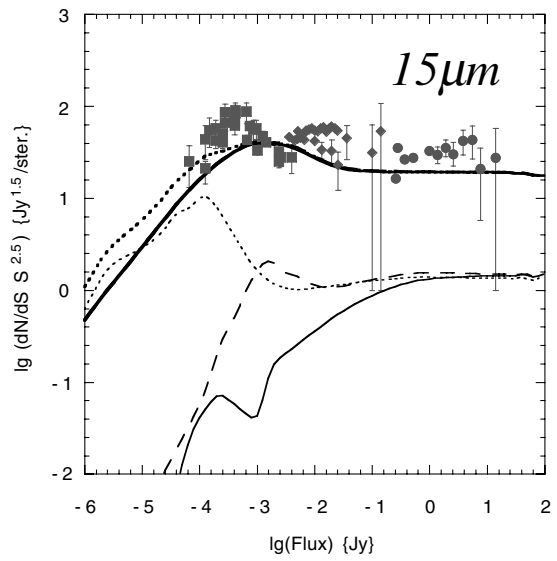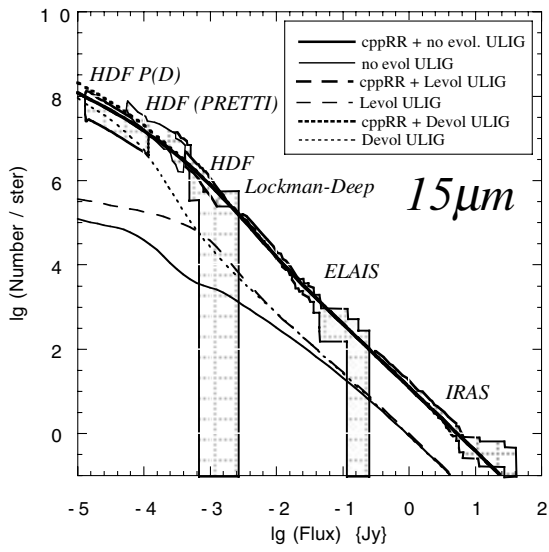
Finally, in the submillimetre at 850 μm, the biggest deficit between the observed and predicted counts is seen. Surveys of both blank fields and around lensed clusters [Smail et al. 1997; Barger et al. 1998; Hughes et al. 1998; Eales et al. 1999] of areas ranging from 0.002–0.12 deg^2, from 1–8 mJy have revealed source densities up to three orders of magnitudes above no-evolution predictions. Furthermore, as a result of the steep K-corrections in the submillimetre, the flux of high-redshift galaxies is enhanced, resulting in almost no difference in the ability to detect a galaxy with a redshift of between 1 and 10. However, even at 850 μm we also see that monotonically increasing power-law density evolution cannot fit the counts and produces too much evolution at higher redshift. Blain et al. (1998) concurred with this result by finding that fitting the counts with pure density evolution would result in a violation of the background radiation by two orders of magnitude. Interestingly, however, it is the luminosity evolution model that comes tentatively close to the observed source counts at the brightest and faintest fluxes.

From Fig. 4 it is apparent that significantly drastic evolution, in both magnitude and form, will be required to fit the observed source counts. From the fits to the faint ends of the 170-, 850- and marginally to the 15-μm counts, significant density evolution at high redshifts seems unlikely. Also, exceeding the observed source counts at 170 and 850 μm, such density evolution would also violate the constraints set by the FIR background radiation. Matsuhara et al. (2000) found that the integral counts at 170 μm in the Lockman Hole at a flux of ∼150 mJy had a steep slope, $\log(dN/dS) = \alpha \log S, \alpha \approx -3$. However, they summarized that if this slope did not become shallower before ≈1 mJy then the power in the calculated fluctuation spectrum would exceed the observed power by a factor of 10. Therefore at some point the source counts must flatten to a value of $\alpha < -2$. Fig. 4 shows that by assuming monotonically increasing density evolution to $z \approx 2.5$, the counts remain steep down to fluxes fainter than 1 mJy. At 850 μm, constraints set by *COBE* measurements of the submillimetre background radiation (Fixsen et al. 1998; Hauser et al. 1998) require that the SCUBA submillimetre counts must converge at fluxes ∼ 0.3–0.5 mJy (Hughes et al. 1998; Hughes 2000a). Again, assuming power-law density evolution, the counts remain steep down to fluxes deeper than 0.1 mJy. Observations and follow-ups of the *ISO* 15-μm surveys of the CFRS, HDF, Lockman Hole and Marano fields identified the sources with galaxies at redshifts of between 0.3 and 1 with a median redshift of ≈0.8 (Mann et al. 1997; Elbaz et al. 1999; Flores et al. 1999a).

In summary, there is too little density evolution at low redshift ($z \sim 1$), and too much density evolution at high redshift ($z \sim 2$) in the power-law evolution parametrization to fit the observed source counts at far-IR and submillimetre wavelengths. Furthermore, the 15 and 170-μm counts require extreme evolution from a redshift of ≈0.2 (the limit of *IRAS*) to ≈1. On the other hand, the SCUBA 850-μm counts and the 170-μm fluctuation analysis will constrain the upper redshift limit on the evolution. Therefore, I assume that the ISOCAM 15-μm differential counts can provide a good
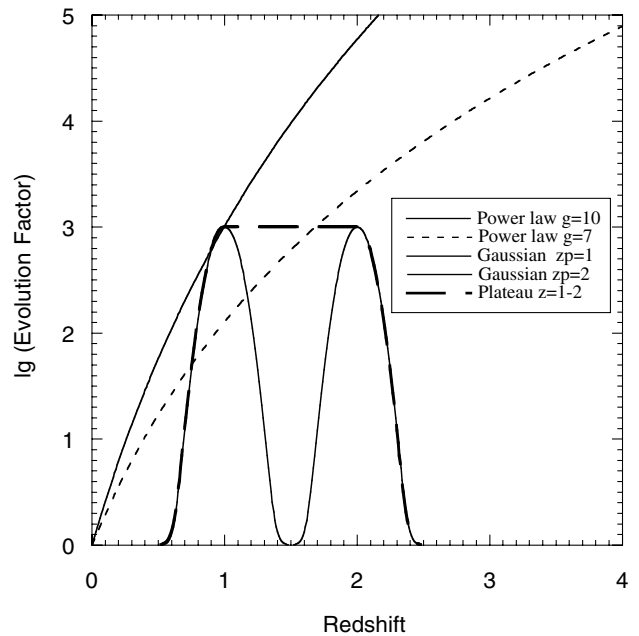

Figure 5. Density evolution parametrizations for the ULIG component models discussed in the text. Density evolution is investigated via three exponential models. Two Gaussian parametrizations peaking at a redshift of 1 and 2, respectively, plus an exponential plateau model ranging from $z = 1$ to 2 are shown. Also shown for comparison are classical power-law density evolution models with power indices $g = 10$ and 7 (i.e. those previously assumed for the classical density evolution of *IRAS* sources, see Fig. 4), respectively. The magnitude of the density evolution in the $z_p = 1$ Gaussian scenario is equivalent to the magnitude of the evolution in the power-law model using a value of $g = 10$ at $z = 1$.

boundary to constrain the evolution in the low-redshift Universe ($0 < z < 1$), and the 850-μm SCUBA submillimetre counts will constrain the evolution in the high-redshift Universe ($1 < z \sim 3$). The evolution of the galaxy population will also be constrained at high redshifts by the measurements of the cosmic infrared background (CIRB). By simultaneously examining evolution scenarios that successfully fit both the 850- and 15-μm counts it is expected that the model fits to the data at intermediate wavelengths and CIRB will also converge.

3.3 Density evolution analysis

Treating only the ULIG component, in order to investigate the density evolution, I consider three simple Gaussian models (see Fig. 5; although not exponential in the strictest sense, hereafter referred to as exponential evolution). Narrow Gaussian profiles peaking at a redshift of 1 and 2 are compared with each other and also with a scenario, referred to as the Gaussian plateau, similar to the anvil model of Blain et al. (1999b), that evolves exponentially to a redshift of ∼1 and declines exponentially after a redshift of ∼2.

Figure 4. Comparison of source counts including the luminous/ultraluminous IR galaxy (ULIG) component assuming the cppRR framework for the normal, starburst and AGN components. Integral and differential counts at 15, 60, 170 and 850 μm are shown for three classic evolution scenarios of the luminous/ultraluminous IR galaxy component (thin lines). Also shown is the total contribution of all components including the ULIG component (thick lines) and a non-evolving ULIG component (solid lines). Pure luminosity evolution of the form $f(z) = (1 + z)^{3.1}$ (Levol – dashed lines) and pure density evolution of the form $g(z) = (1 + z)^7$ (Devol – dotted lines). Data is from 15 μm – Oliver et al. (1997), Aussel et al. (1999), Elbaz et al. (1999) and Serjeant et al. (2000)., 60 μm – Hacking & Houck (1987), Lonsdale et al. (1990), Rowan-Robinson et al. (1990), Saunders (1990) and Gregorich et al. (1995)., 170 μm – Kawara et al. (1998), Puget et al. (1999) and Matsuhara et al. (2000) [fluctuation analysis – dotted box]; 850 μm – Smail et al. (1997), Hughes et al. (1998), Barger et al. (1999a), Blain et al. (1999a) and Eales et al. (1999).

The Gaussian profiles have the form,

$$D(z) = 1 + g \exp\left[-\frac{(z - z_p)^2}{2\sigma^2}\right], \tag{7}$$

with the peak magnitude of the evolution, $g = 1000$, the Gaussian width (effectively the evolution time-scale) $\sigma = 0.1$, and the peak redshift $z_p = 1$ and 2, respectively. The Gaussian plateau model assumes an exponential increase and decrease as equation (7), to and from redshifts of 1 and 2 respectively, and a constant value of $1 + g$ in between. Although these models are merely intended to highlight the effect of density evolution at different redshifts, the narrow Gaussian profiles may be considered as epochs of short, intense merging while the Gaussian plateau represents a longer episode of galaxy merging (and consequent star formation/galaxy IR emission).

Using these density evolution scenarios, the correspondingly evolving ULIG components are re-plotted in Fig. 6 at 15 and 850 μm. Several points are worth noting in comparison with Fig. 4. Assuming the exponential evolution from equation (7), a value of $g = 1000$ at redshift $= 1$ corresponds roughly to a $g \sim 10$ in the $(1 + z)^g$ power-law scenario with the significant difference that the high-redshift density evolution has vanished. The 15-μm counts remain relatively unchanged since they are not so sensitive to any density evolution at high redshift ($z > 1$). However, the effect on the 850-μm submillimetre counts is significant in that the excess at the faint fluxes (~ 1 mJy) has disappeared. In the case of the $z_p = 2$ scenario, the 15-μm counts cannot be fitted because of the fact that there is no evolution at lower redshift where it is needed. In fact, as can be seen from the Gaussian plateau model, the 15-μm counts in general are clearly insensitive to density evolution at higher redshifts ($z > 1$). From the 15-μm counts, it is clear that power in the local density evolution is required. For the 850-μm counts (Fig. 6), density evolution peaking at either $z = 1$ or 2 is acceptable. However, the Gaussian plateau model, with constant density evolution from $z = 1$ to 2 violates the faint end of the 850-μm counts.

3.4 Luminosity evolution analysis

Despite the apparent success at 15 μm, the brighter SCUBA counts at 850 μm ($S > 1$ mJy) seem impossible to fit with this form of density evolution alone. Even the evolved counts still fall too far to the left and low in the log(N)/log(S) plane when compared to the observations > 1 mJy. In general, the brighter SCUBA population is composed of fewer but more powerful sources (a high-redshift 8-mJy SCUBA source being approximately 10 times more luminous than the most luminous local sources). Additional clues come from a further inspection of the luminosity evolution models of Fig. 4. In general the addition of luminosity evolution has the generic effect of shifting the source counts towards brighter fluxes [to the right of the log(N)/log(S) plane as the brighter, evolved sources are seen at lower sensitivities, i.e. higher flux values].

Therefore, I extend the analysis of the density evolution scenarios to include a similar subset of luminosity evolution models. Following the same doctrine as the density evolution analysis I define the luminosity evolution as,

$$L(z) = 1 + k \exp\left[-\frac{(z - z_p)^2}{2\sigma^2}\right], \tag{8}$$

with the magnitude of the evolution, $k = 5$, $\sigma = 0.3$, $z_p = 1$ and 2, respectively. Thus this form would be equivalent to a value of
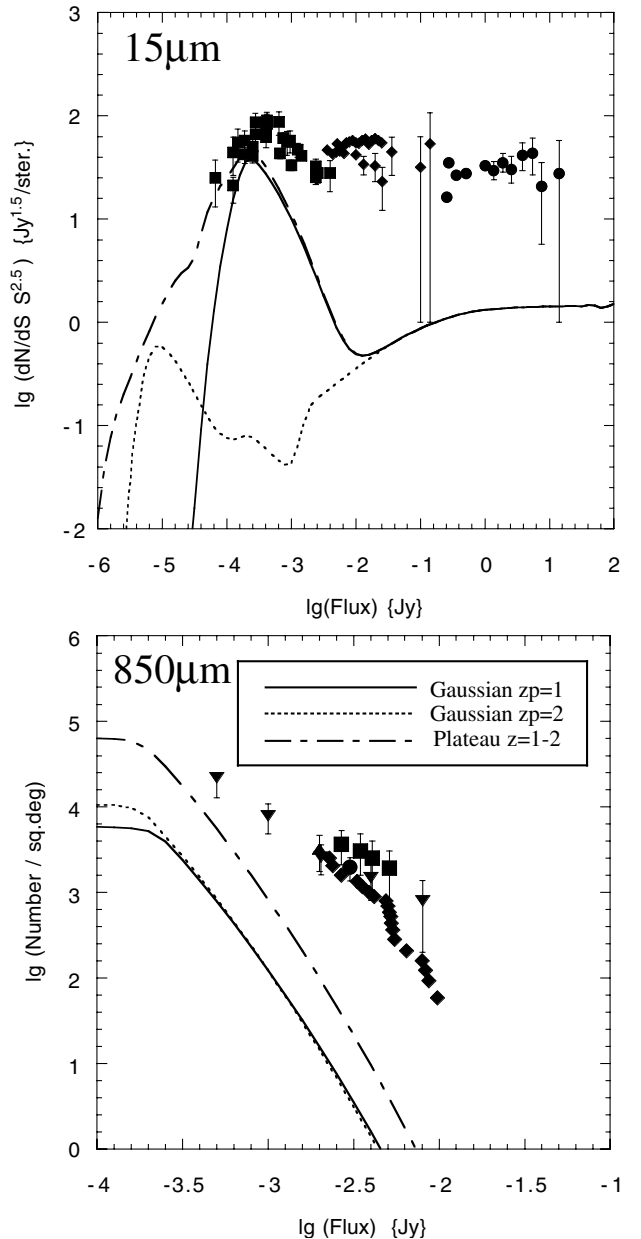

Figure 6. Source counts of the high-luminosity component only at 15 (differential) and 850 μm (integral), respectively. The three model lines correspond to the three exponential density evolution scenarios of the ULIG component discussed in the text. References for the observed points are given in the text and figures.

$k \sim 2.3$ for the case of the $(1 + z)^k$ power-law luminosity evolution. Note the disparity in the magnitude/width of the luminosity and in the density distributions. First, it should be noted that the luminosity and density evolution enter the cosmological equations differently. Density evolution increases the number of sources observed in a given volume defined by a sensitivity $S(z)$ and redshift, z. The volume remains the same and the number density of sources increase. On the other hand, the effect of luminosity evolution is to increase the observable volume via a lowering of $S(z)$ while preserving the source number density. Furthermore, the luminosity evolution analysis is performed on the assumption of there already being the presence of density evolution at low redshift manifested as the $z_p = 1$ exponential density evolution scenario.
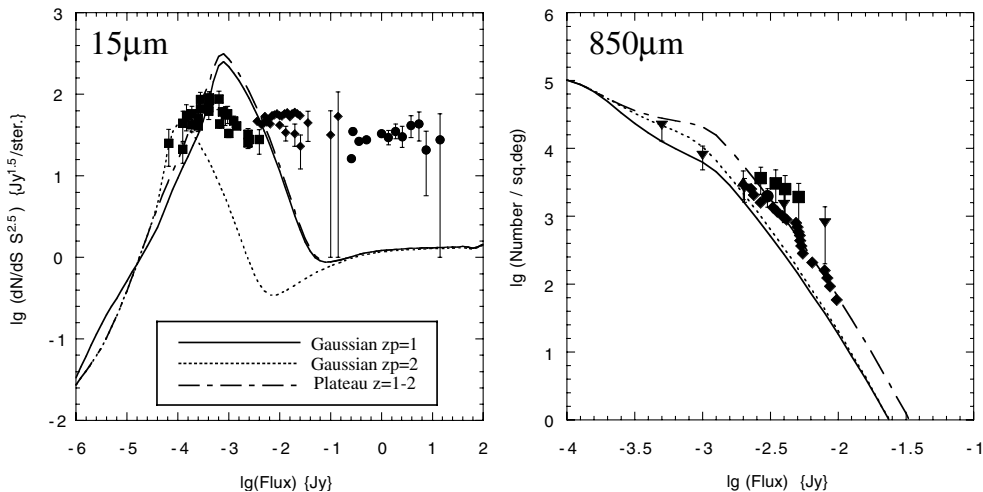
Figure 7. Source counts of the high-luminosity component only at 15 (differential) and 850 μm (integral), respectively. The three model lines correspond to the three exponential luminosity evolution scenarios discussed in the text. Note that the low-redshift density evolution scenario is also assumed and included in these plots. References for observed points are given in the text and figures.

Fig. 7 shows the differential and integral counts of the ULIG component at 15 and 850 μm, respectively, for the three luminosity evolution scenarios described by equation (8). In this analysis, a density evolution of the form in equation (7) is assumed with parameter values of $g = 500$, $\sigma = 0.1$ and $z_p = 1$. As expected, the addition of the luminosity evolution moves the counts to the right in the log(N)/log(S) plane.

At 15 μm, evolution at higher redshift ($z_p = 2$) is not well constrained by the counts, as the 15-μm sources are in general expected to reside at lower redshift. The $z_p = 1$ Gaussian and plateau (as a result of the $z \sim 1$ contribution) scenarios strongly violate the differential counts at 15 μm, not because of the strength of the luminosity evolution alone, but in fact more because of the superposition of both the luminosity and the density evolution effects at these redshifts. The 15-μm differential counts put a severe constraint on the magnitude of the luminosity evolution at lower redshift in the presence of density evolution.

At 850 μm, the effect of the addition of luminosity evolution is spectacular. The shift to the right in the log(N)/log(S) plane can effectively fit the SCUBA counts at fluxes both fainter and brighter than 2 mJy. There is little difference between the high- or low-redshift evolutionary scenarios, implying that many of the SCUBA sources are at redshifts higher than unity, allowing the $z_p = 2$ scenario to compete with the combined effect of the luminosity and density evolution in the $z_p = 1$ scenario. However, it should be noted that there is a significant difference between the two Gaussian scenarios and the plateau scenario. It would seem that constant luminosity evolution over the entire redshift range $z = 1$–2 is ruled out by the count constraints.

As with the density evolution analysis, the SCUBA 850-μm counts are constrained by the evolution at higher redshift while the 15-μm counts are severely constrained at lower redshift. This bipolar constraint is highlighted in the way the plateau curve hugs the $z_p = 1$ Gaussian luminosity evolution curve at 15 μm, while at 850 μm there is a more clearer superposition of the two Gaussian scenarios.

4 CONSTRUCTION OF NEW EVOLUTIONARY MODELS

4.1 Source counts

From the analysis of the effects and constraints on the density and

luminosity evolution of the IR high luminosity population (assumed to be ULIGs) in the previous section, the following points/constraints can be considered,

(i) The evolution can be constrained by simultaneous consideration of the 15- and 850-μm counts.

(ii) The 15-μm counts are predominantly dominated by low-redshift galaxies and insensitive to the high-redshift population.

(iii) The faint end of the 850-μm counts constrains the amount of density evolution allowed.

(iv) Simple density evolution scenarios can fit the 15-μm counts but are unable to account for the submillimetre counts at fluxes >2 mJy.

(v) The addition of luminosity evolution has the effect of moving the source counts towards brighter fluxes in the log(N)/log(S) plane.

(vi) The 15-μm counts place strong constraints on the luminosity evolution at low redshift but are insensitive to luminosity evolution at higher redshifts.

(vii) Luminosity evolution at either high or low redshift can fit the 850-μm counts (i.e. the SCUBA counts effectively only constrain the magnitude of the luminosity evolution in this scenario).

From these considerations a model can be envisioned that includes both density evolution at lower redshift (peaking at $z \sim 1$) and luminosity evolution peaking at higher redshift. The exact details of the evolution are constrained by fits to the source counts, which will depend on both the magnitude of the evolution and the degree of overlap in the redshift space between the tails of the density and luminosity evolution. The magnitude of the evolution at high redshift will ultimately be constrained by the CIRB.

Using these three constraints (15-μm differential counts, 850-μm integral counts and the CIRB) and the results from the previous analysis, the following evolutionary scenario is presented. The basic framework of the cppRR model is retained with the galaxy population consisting of four main components. Normal (cirrus) galaxies are represented by the cool 60-μm *IRAS* luminosity function and are essentially non-evolving although a gradual decline towards higher redshift is included to represent gradual formation and/or transition through a starburst phase. The
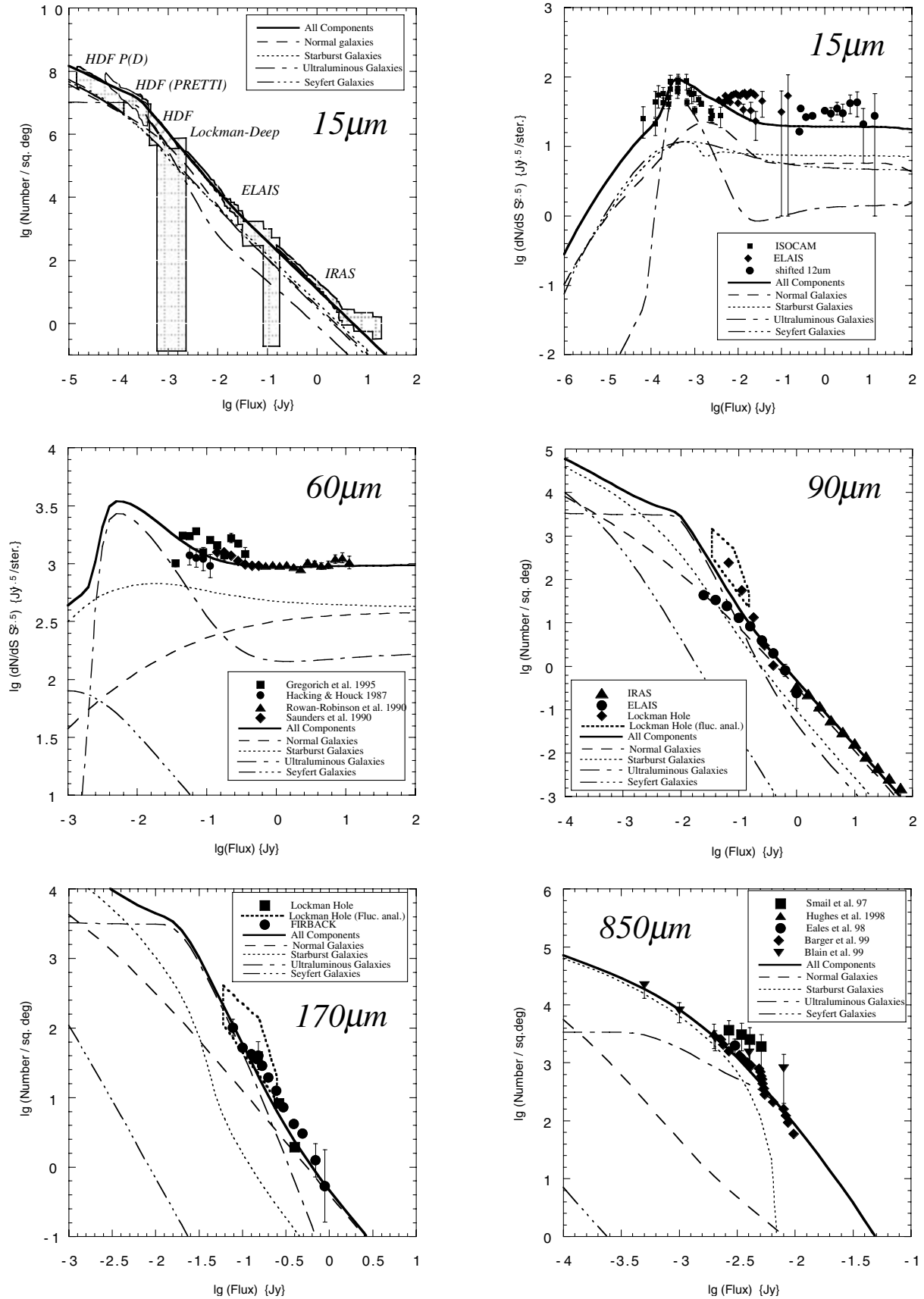
Figure 8. Integral and differential counts at 15, 60, 90, 170 and 850 μm for the new evolutionary model of normal, starburst, ultraluminous and Seyfert galaxies as described in the text. Data is from 15 μm – Oliver et al. (1997), Aussel et al. (1999), Elbaz et al. (1999) and Serjeant et al. (2000); 60 μm – Hacking & Houck (1987), Rowan-Robinson et al. (1990), Saunders (1990) and Gregorich et al. (1995)., 90 μm – Matsuhara et al. (2000a) (fluctuation analysis – dotted box) and Efstathiou et al. (2000). 170 μm – Kawara et al. (1998), Puget et al. (1999) and Matsuhara et al. (2000) (fluctuation analysis – dotted box). 850 μm – Smail et al. (1997), Hughes et al. (1998), Barger et al. (1999a), Blain et al. (1999a) and Eales et al. (1999).

warm *IRAS* galaxies (starbursts) and Seyfert galaxies are represented by the 60- and 12-μm *IRAS* luminosity functions respectively, and evolve in luminosity at a rate $\propto (1 + z)^{3.2}$ to $z = 2.5$ and then gradually decline at higher redshifts thus eliminating the artificial cut-off employed previously in the cppRR model and pointed out by Rowan-Robinson (2000) as being a general shortcoming with many models employing the backward evolution approach to galaxy evolution. Choosing a peak in the luminosity evolution at high redshift ($z = 2.5$) is consistent with the higher redshift galaxies contributing more to the counts/ background at longer wavelengths (Gispert, Lagache & Puget 2000). The high-luminosity end of the IR 60-μm luminosity function, the LIG/ULIG component, $\log L^{*}_{60\mu m} \sim 11.6 \, L_{\odot}$, evolves in both number density and luminosity. The density evolution is strong and exponential, following equation (7) peaking at a redshift of 1 with the magnitude of the evolution, $g = 220$ and Gaussian width, $\sigma = 0.25$. The luminosity evolution rises exponentially as equation (8) with a magnitude $k = 40$, $\sigma = 0.58$ to a maximum redshift, $z_p = 2.5$ and then slowly declines exponentially to higher redshifts. The magnitude of the luminosity evolution at the peak redshift in the starburst, Seyfert and ULIG components is similar, although the latter suffers a steeper decline towards lower redshift reflecting the more violent star formation within these galaxies.

Fig. 8 shows the fits of the new evolutionary model to the source counts as observed by *ISO* (15, 90 and 170 μm), *IRAS* (60 μm) and SCUBA (850 μm). The new model incorporating the strongly evolving LIG/ULIG component fits the observed counts extremely well with the LIG/ULIG component accounting for the bumps in the 15-μm counts at 0.1–1 mJy, the rise towards fainter fluxes in the 60-μm differential counts, the excesses at 90 and 170 μm and much of the SCUBA population brighter than 2 mJy at 850 μm. At 170 μm Matsuhara et al. (2000) concluded, on the basis of the 170/ 90 μm colours of galaxies in their Lockman Hole field, that the faint sources could not be cirrus dominated (normal galaxies) but had to be star-forming systems, consistent with the model prediction of a change in the dominant population, from cirrus to star-forming ULIGs at ~400 mJy. Note that there is still a significant discrepancy between the 90-μm *ISO* source counts conducted by the Japanese team (Kawara et al. 2000; Matsuhara et al. 2000) and the European Large-Area *ISO* Survey (ELAIS; Efstathiou et al. 2000). The model conservatively predicts a value between these two estimations.

4.2 Number redshift distributions

Figs 9, 10 and 11 show number redshift distributions for the new evolutionary model at 15, 170 and 850 μm, respectively.

The numerous *ISO* surveys at 15 μm have a general consensus with a strong evolution of sources to $z \sim 1$, with the corresponding redshift distribution peaking in the range $z \sim 0.7$–1.0 (Elbaz 1999b). The *N–z* distributions in Fig. 9 are broadly consistent with this strong evolution although there is a double peak in the distribution because of the form of the assumed evolution. The lower redshift peak is a result of the normal galaxies that dominate the source counts to ≈ 1 mJy. As the *N–z* distribution probes to fainter fluxes, the contribution from the ULIG population (centred around $z \sim 1$) increases. These models serve to show the effect of a strongly evolving population to $z \sim 1$ on the source counts, and moving the peak of the density evolution to lower redshift or increasing the Gaussian width of the evolution would produce a smoother *N–z* distribution effectively merging the two peaks.

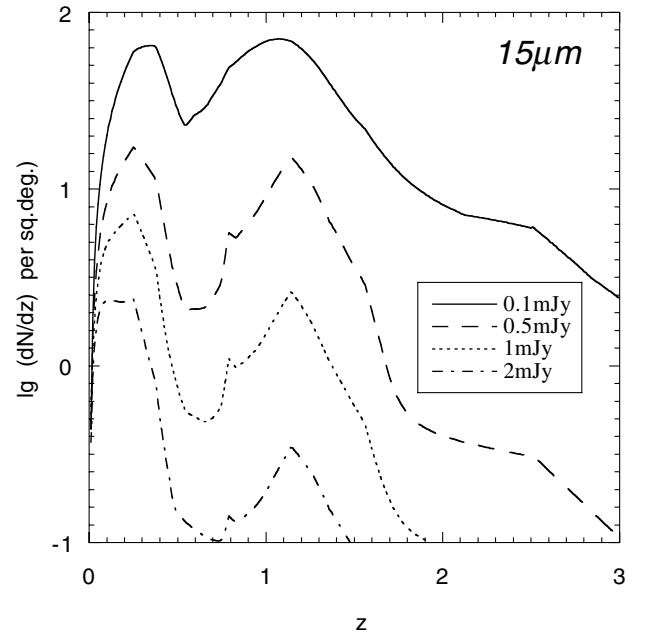At 850 μm, the redshift of the detected sources is notoriously

Figure 9. Number–redshift distributions at 15 μm for all components in the model for fluxes ranging from 0.1 to 2 mJy. The peak at the lowest redshifts is a result of the normal galaxy population. The ULIG population dominates at $z \sim 1$.
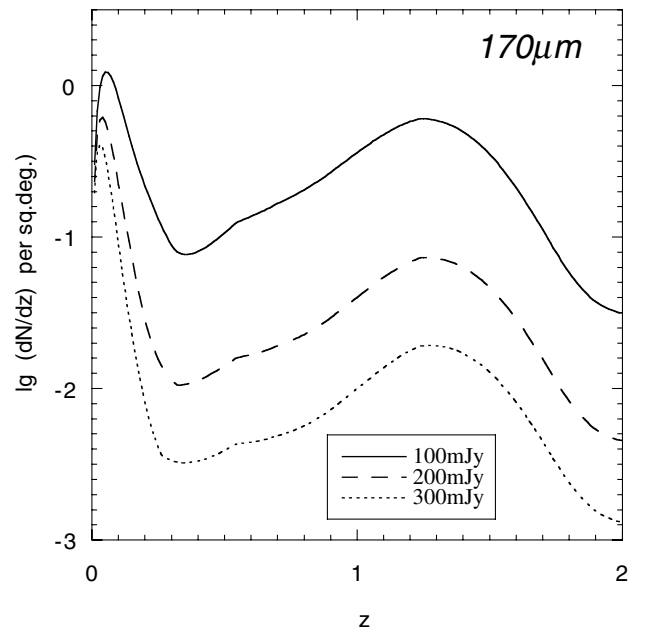

Figure 10. Number–redshift distributions at 170 μm for all components in the model for fluxes ranging from 100 to 300 mJy. The peak at low redshifts ~ 0.1 is because of normal galaxies. Note that the *N–z* distribution is measured as d*N*/d*z*, therefore although the peak because of normal galaxies is high, the width of its distribution is narrow.

difficult to measure unambiguously, the main problem being the 2–3 arcsec (or more) positional uncertainty in the submillimetre observations for a 15-arcsec resolution at 850 μm (Hughes 2000b). Furthermore, there is often only a single definite detection at 850 μm in the entire spectral range from the submillimetre to the far-IR ~200 μm. SCUBA preferentially selects galaxies at redshift >1 because of the shape of the SED of galaxies in the
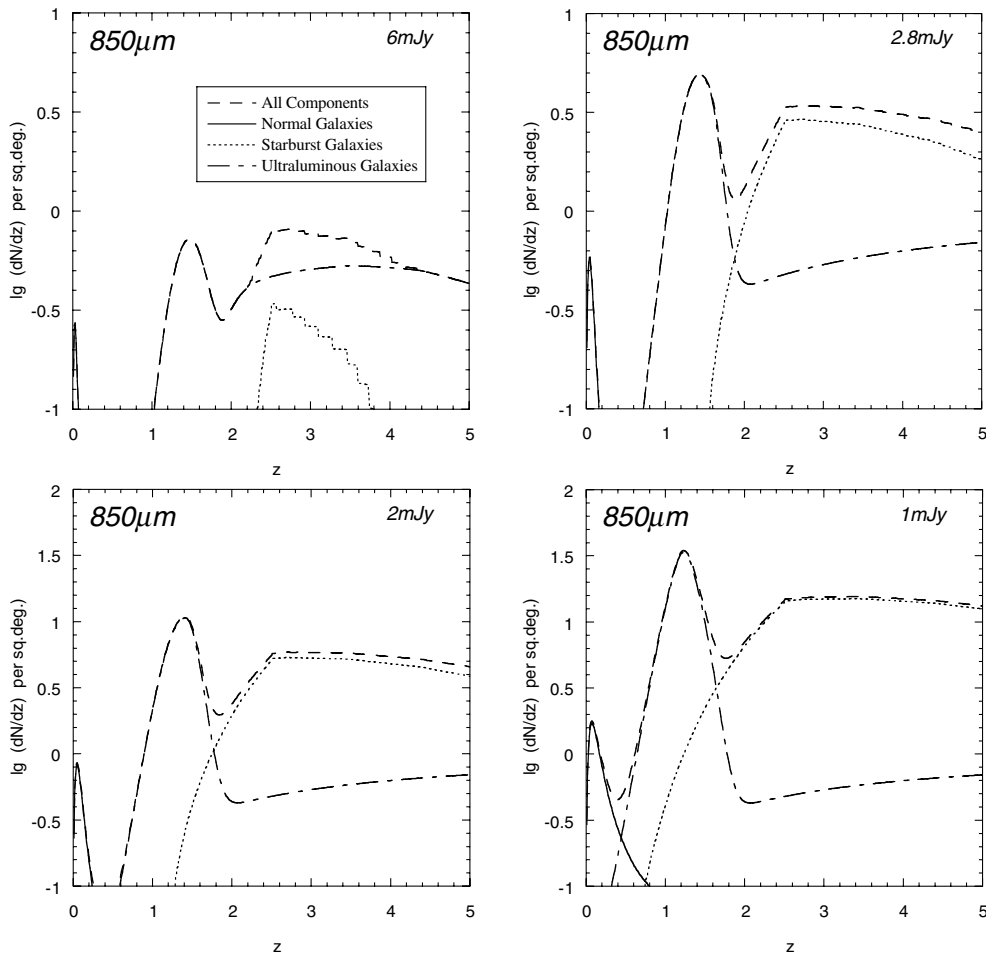
Figure 11. Number–redshift distributions at 850 μm for individual components in the model for fluxes ranging from 1 to 6 mJy. In general, the normal galaxies are represented by the low-redshift peak in the N–z distribution.

submillimetre regime. A spectroscopic survey by Barger et al. (1999b) of a lensed submillimetre sample (Smail et al. 1999) concluded that the submillimetre population resided mainly between $z \approx 1$ and 3 with a median redshift between 1.5 and 2. For the three SCUBA galaxies for which there are CO spectroscopy confirmed redshifts, all lie at $z > 1$ (Frayer, Tvison & Scoville 1998, 1999; Soucail et al. 1999). However, the first identifications from the Canada–UK deep submillimetre survey have shown that the SEDs of the submillimetre sources (0.8, 15, 450, 850 μm and 6 cm) are consistent with high IR luminosity Arp 220 type luminous IR galaxies, many undergoing mergers/interactions with $\approx 1/3$ of the sample at $z < 1$, $1 < z < 3$ and $z > 3$, and a slightly higher median redshift of ~ 2 (Lilly et al. 1999). Eales et al. 1999. Eales et al. 2000 combined the Canada–UK deep survey, lensed surveys and HFF survey (Barger, Cowie & Richards 2000), producing a combined median redshift of 2.41. Finally Smail et al. (2000) using the method of Carilli & Yun (1999, 2000; see also Dunne, Clements & Eales 2000b) combined radio data for a submillimetre sample to fit radio-submillimetre SEDs, thus obtaining rough estimates of redshifts and finding a median redshift between 2 and 3 for the submillimetre sources brighter than 1 mJy. In general the trend is for a spread of redshifts between 1 and 3 and higher with a median around $z \gtrsim 2$. Fig. 11 is broadly consistent with these estimates. At the brightest fluxes (~ 6 mJy) the redshift distribution is dominated by the ULIG galaxy population, consistent with the SCUBA observations of bright sources. In

this region the evolution is dominated by the higher redshift luminosity evolution component. As the redshift distribution is sampled towards lower fluxes, two points are worth noting. The first is the emergence of the starburst galaxy population as the dominant contributor at high redshift and the second is the strengthening of the number evolution component of the ULIG population.

4.3 Background radiation

Further constraints on the evolutionary model come from the CIRB which manifests itself as the superposition of the unresolved population of faint sources in the Universe. The far-IR background has been well constrained from ~ 100 μm–2 mm by measurements made using the FIRAS/DIRBE instruments on *COBE* (Puget et al. 1996; Fixsen et al. 1998; Hauser et al. 1998) and from the *ISO* source count fluctuation analysis at 240–140 μm (Puget et al. 1999; Matsuhara et al. 2000). Finkbeiner, Davis & Schlegel (2000) have also reported possible detections and an excess at 60 and 100 μm. In the submillimetre, lensed counts to 0.5 mJy have discovered enough sources to approximately account for the 850-μm background of $\nu I_\nu = 5 \times 10^{-1}$ nW m^{-2} sr^{-1} (Blain et al. 1999a). In Fig. 12, contribution of the new evolutionary model to the CIRB is shown compared with the observations described above.

The model lies comfortably within the upper and lower constraints set by FIRAS. The cosmic background peaks at ~ 140 μm where detections by both Hauser et al. (1998) and the
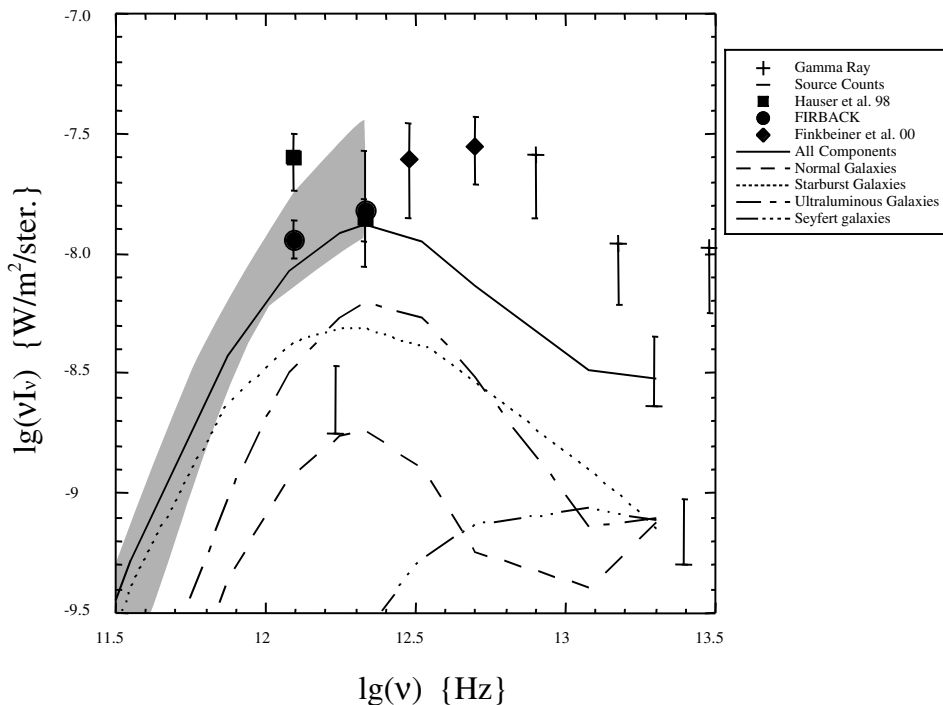
Figure 12. The contributions to the infrared-submillimetre background light predicted by the model. The shaded area in the figure represents the constraints set by the FIRAS experiment on *COBE*. Source Counts refers to lower limits set from the integrated light of galaxy source counts. Gamma ray refers to limits set by the attenuation of TeV gamma rays by the background radiation. *FIRBACK* refers to the integrated light of galaxies calculated from the FIRBACK survey (Puget et al. 1999).

FIRBACK survey (Lagache et al. 1999) are in good agreement. Note that the longer wavelength (240-μm) measurements of *COBE* and FIRBACK do not agree so well although Lagache et al. (1999) assumed a significant correction arising from the warm interstellar dust (WIM) in their calculations. The model matches both the position and the magnitude of this peak extremely accurately. One direct consequence of this is that the majority of this peak emission would be expected to come from relatively low-redshift galaxies (Gispert et al. 2000). The evolution in the high-redshift regime is strongly constrained by the CIRB/submillimetre background at longer wavelengths where the CIRB slope is shallower than the average galaxy SED, implying a strong contribution from the integrated light of high-redshift sources where the peak of the IR-SED is being sampled in the submillimetre waveband. It should be noted that assuming an $\Omega = 1$ cosmology results in an extremely marginal fit to the longer wavelength (submillimetre–mm) regime.

Constraints on the CIRB at shorter wavelengths come from Diffuse Infrared Background Experiment (DIRBE), *Infrared Telescope in Space* (*IRTS*; Matsumoto et al. 2000), galaxy source counts and TeV gamma rays (Stecker 2000), although the source count measurements and background measurements are yet to converge on an agreed value probably because of the difficulty in ascertaining the correction factor arising from the zodiacal light that peaks at ~25 μm (Ozernoy 2000).

Although the peak of the CIRB is well explained by the strongly evolving ULIG population in this model, the stronger contributors at submillimetre wavelengths are in fact the starburst galaxies. Furthermore, although much of the submillimetre background may be made up from a population of ULIG galaxies (30–50 per cent being resolved into individual galaxies with $S_{850} > 2$ mJy), the surface density of the submillimetre population is significantly higher (Hughes 2000b). Note that Eales et al. (2000) have pointed

out that the SCUBA fluxes may be upwardly biased by a factor of 1.4 as a result of source confusion and noise, resulting in a reduction of the resolved CIRB at 850 μm to 20 per cent.

Such models of the CIRB are also consistent with the 850-μm source counts (see Fig. 8). The ULIG component is completely dominant at bright fluxes down to ~6 mJy. Below this limit the starburst galaxies begin to contribute more strongly, where at $S_{850} < 2$ mJy they become the dominant source population. Peacock et al. (2000) made a statistical analysis of the 850-μm SCUBA map of the *Hubble Deep Field* (HDF) estimating that as much as 48 per cent of the CIRB at 850 μm could come from the submillimetre emission from the UV star-forming galaxies with 30 per cent from ULIGs (Hughes et al. 1998) and a further 10 per cent from AGN (Almaini, Lawrence & Boyle 1999). If the starburst population in the model is literally taken as the equivalent of the UV galaxies in the HDF, then the model predictions slightly overpredict this contribution from the starburst galaxies, although the transition between starburst–LIG–ULIG is not clearly defined and therefore has a large scope for interpretation. The submillimetre source counts are also consistent with the results of Chapman et al. (2000) who carried out a submillimetre survey of 33 Lyman break galaxies (Madau et al. 1996) to ~1.3 mJy. The average flux of these sources was found to be $S_{850} \sim 0.6$ mJy implying that they would occupy the fainter end of the submillimetre source counts and would not significantly contribute to the brighter $S_{850} \sim 5$ mJy source counts. Therefore it would seem that at the brighter submillimetre fluxes (2–5 mJy) we are observing the ULIG population where as much as one third of the CIRB at 850 μm can be resolved into individual bright sources. The underlying fainter population is distinct from the ULIGs and is more akin to the UV Lyman break galaxies and/or *IRAS* starburst galaxies. In this scenario the 850-μm counts are a superposition of two galaxy populations, starbursts and ULIGs.

5 DISCUSSION

The aim of this work has been to find an evolutionary model that can viably fit the galaxy source counts from the mid-IR to submillimetre without violating the constraints set by the IR background and CMB measurements, and this was not born from a fundamental physical assumption. The predicament of the model discussed in this paper is about how the bimodal evolution (i.e. dual evolution) manifests itself in the evolutionary history of a galaxy. Are we observing a representation of two stages of galaxy evolution of the same population or different evolutionary paths of separate populations? Of the 19 SCUBA sources detected at 850 μm in the Canada–UK submillimetre survey, only two were found to have *ISO* 15-μm associations implying that the *ISO* and SCUBA sources are in fact different populations, (or different redshift regimes; Eales et al. 2000). Furthermore, what role do the ULIGs play in the evolutionary history of AGN? Do all QSOs go through a dusty ULIG phase, considering that the space density and luminosities of QSOs and ULIGs in the local Universe are similar (Soifer et al. 1987a).

If this scenario is considered as two phases of evolution then the initial formation of the core (collapse of dark-matter halo) would take place at high redshift accompanied by the initial formation of a black hole and associated star formation slowly declining towards lower redshift as the initial fuel is used up. The peak in the comoving number density of AGN is at a redshift of ~ 2; at lower redshifts these AGN are found to be hosted in gE galaxies (McClure et al. 1999). Thus the mid-IR 3–30 μm SED may be indicative of the galaxies merging at lower redshifts activating/re-activating the central black hole where at some time the buried AGN expels the surrounding dust becoming the dominant energy source. The SED > 50 μm remains starburst dominated. The ULIGs would undergo rapid evolution from high redshift eventually evolving into todays local gE galaxies. Local giant ellipticals gE galaxies are the only local systems with core densities high enough ($100 \, M_\odot \, pc^{-3}$) to account for a past ULIG evolutionary phase (Kormendy & Sanders 1992; Binggeli 1994; Trentham 2000.

6 CONCLUSIONS

The backward evolution approach to galaxy evolution has been re-visited in the light of recent observations by *ISO* and SCUBA in the infrared and submillimetre regions. Assuming classical evolutionary scenarios incorporating power-law luminosity and density evolution it is impossible to simultaneously fit all the source counts from 15–850 μm and the CIRB.

A new evolutionary model is investigated which assumes the foundations of the cppRR model. In addition to this original framework, a strongly evolving high luminosity IR galaxy component (referred to as the ULIG component but specifically the high-luminosity end of the 60-μm luminosity function) is added. This new population evolves in both density and luminosity and is capable of fitting both the source counts from 15–850 μm and the cosmic far-IR background radiation, including the peak at ≈ 140 μm and the long-wavelength tail.

In this scenario the ULIG component is tenuously interpreted as the progenitor of the present-day gE galaxy population.

The excesses in the 15- and 170-μm counts are well explained by strong evolution to redshift ~ 1 of a population of luminous, $\log L_{IR} \sim 12 \, L_\odot$, infrared galaxies. This population of galaxies becomes prominent at flux levels just below the limits of the *IRAS*

60-μm survey (although previously hinted at) and can be associated with the archetypical ULIG Arp220. These results are generally consistent with the numerous surveys at 15 μm (Elbaz 2000) which found that the dominant population above a redshift of ~ 0.5 was massive ($M > 10^{11} \, M_\odot$, luminous $L_{IR} > 10^{11-12} \, L_\odot$ galaxies).

At 850 μm, these galaxies dominate the bright SCUBA counts at $S \gtrsim 6$ mJy. Towards fainter fluxes the starburst galaxies begin to contribute strongly to the source counts, becoming dominant at fluxes < 2 mJy. In this scenario the submillimetre counts can be divided into two distinct populations, the dusty, giant ULIGs which would be considered the progenitors of gE galaxies and the *IRAS* starburst population/Lyman break galaxies. This conclusion is in good agreement with the analysis of Busswell & Shanks (2001) who transformed the optical counts of faint starburst galaxies to the submillimetre waveband. Using a Bruzual & Charlot (1993) galaxy model with an exponentially decaying star formation rate of $\tau = 9$ Gyr, their models successfully predicted optical results, including the Lyman break galaxies (Metcalfe et al., in preparation). Furthermore they accounted for the submillimetre counts below a sensitivity of ~ 1 mJy but failed to fit the counts at brighter fluxes, concluding that an additional population was required (ULIGs/AGN?). Of further interest is that their models were also deficient in fitting the CIRB at 140–240 μm where the ULIG population is most prominent.

Note, analysis of the so-called Madau plot of the star formation history of galaxies in this evolutionary model will be addressed in a later paper. The primary aim of this work is to ascertain what evolutionary scenarios can successfully fit the observed source counts/background radiation.

From an analysis of the luminosity and density evolution the following conclusions can be drawn from the galaxy source counts.

(i) The mid-IR region (15 μm) is sensitive to evolution in the low-redshift population but is not strongly constrained by evolution at higher redshift ($z > 1$)

(ii) The far-IR region at 60–90 μm does not presently include enough information to constrain the evolution in the source counts.

(iii) The far-IR region at 170 μm is sensitive to the low-redshift population and the faint end counts constrain the contribution to the peak of the CIRB.

(iv) The submillimetre counts constrain the magnitude of the evolution in the high-redshift Universe $z > 1$ but because of the steep *K*-corrections, cannot distinguish evolutionary forms between redshifts 1 and 2.

Using the short wavelength 15-μm and long wavelength 850-μm counts, together with the CIRB as bounding conditions, the evolution over a wide range of both wavelength and redshift can be constrained. It is found that a scenario where the ULIG population undergoes two phases of evolution, a rapid merging epoch to $z \sim 1$ and the exponential evolution in luminosity to higher redshifts, best fits the observations.

In this scenario the high-redshift ULIGs detected at 850-μm fluxes $\gtrsim 2$ mJy may be interpreted as the progenitors of todays gE galaxies while the population at fluxes fainter than $S_{850} \lesssim 2$ mJy represent the *IRAS* starburst population/Lyman break galaxies.

Observations in the next few years in the mid-IR with SIRTF (Rieke 2000) and the Japanese ASTRO-F mission (Matsuhara 1998; Watarai et al. 2000; Pearson et al. 2001), in the far-IR submillimetre–mm with FIRST (Pilbrat 2000), LMT (Schloerb 1997) and an all-sky survey at far-IR wavelengths with ASTRO-F

(Kawada 1998; Takahashi et al. 2000) will undoubtedly solve many of these mysteries.

7 INTERNET ACCESS TO COUNT MODELS

The source count models can be accessed through the world wide web at http://www.ir.isas.ac.jp/~cpp/counts/.

REFERENCES

Acosta-Pulido J. A. et al., 1996, A&A, 315, 121
Almaini O., Lawrence A., Boyle B. J., 1999, MNRAS, 305, L59
Altieri B. et al., 1999, A&A, 343, L65
Archibald E. N., Dunlop J. S., Hughes D., Rawlings S., Eales S. A., Ivison R. J., 2001, MNRAS, 323, 417
Arribas S., Colina L., Borne K. D., 2000, ApJ, 545, 228
Aussel H., Cesarsky C. J., Elbaz D., Starck J. L., 1999, A&A, 342, 313
Barger A. J., Cowie L. L., Sanders D. B., Fulton E., Taniguchi Y., Sato Y., Kawara K., Okuda H., 1998, Nat, 394, 248
Barger A. J., Cowie L. L., Sanders D. B., 1999a, ApJ, 518, L5
Barger A. J., Cowie L. L., Smail I., Ivison R. J., Blain A. W., Kneib J.-P., 1999b, AJ, 117, 2656
Barger A. J., Cowie L. L., Richards E. A., 2000, AJ, 119, 2092
Baugh C. M., Cole S., Frenk C. S., 1996, MNRAS, 283, 1361
Beichman C. A., Helou G., 1991, ApJ, 370, L1
Benn C. R., Rowan-Robinson M., McMahon R. G., Broadhurst T. J., Lawrence A., 1993, MNRAS, 263, 98
Bertin E., Dennefeld M., Moshir M., 1997, A&A, 323, 685
Binggeli B., 1994, in Meylan G., Prugneil P., eds, Proc. ESO Conf. and Workshop, Dwarf Galaxies. ESO Publications, Garching, p. 13
Blain A. W., Longair M. S., 1993, MNRAS, 264, 509
Blain A. W., Smail I., Ivison R. J., Kneib J.-P., 1998, MNRAS, 512, L87
Blain A. W., Kneib J.-P., Ivison R. J., Smail I., 1999a, ApJ, 302, 632
Blain A. W., Smail I., Ivison R. J., Kneib J.-P., 1999b, MNRAS, 309, 715
Bogun S. et al., 1996, A&A, 315, L71
Borne K. D. et al., 1999, ApJS, 266, 137
Borne K. D., Colina L., Bushouse H., Lucas R. A., 2000, ApJ, 529, L77
Boulade O., 1996, A&A, 315, L85
Boyle N., Shanks T., Peterson B. A., 1988, MNRAS, 235, 935
Bruzual A. G., Charlot S., 1993, ApJ, 405, 538
Busswell S., Shanks T., 2001, MNRAS, 323, 67
Carilli C. L., Yun M. S., 1999, ApJ, 513, L13
Carilli C. L., Yun M. S., 2000, ApJ, 5130, 618
Chapman S. et al., 2000, MNRAS, 319, 318
Clements D. L., Sutherland W. J., Saunders W., Efstathiou G. P., McMahon R. G., Maddox S., Lawrence A., Rowan-Robinson M., 1996, MNRAS, 279, 459
Cole S., Aragon-Salamanca A., Frenk C. S., Navarro J. F., Zepf S. E., 1994, MNRAS, 271, 781
Colina L., Arribas S., Borne K. D., Monreal A., 2000, ApJ, 533, L9
Condon J. J., 1994, ApJ, 287, 461
Dole H. et al., 2000, in Lemke D., Stickel M. K., eds, *ISO* Surveys of a Dusty Universe. Springer-Verlag, Tegernsee, p. 54
Dunne L., Eales S., Edmunds M. G., Ivison R., Alexander P., Clements D. L., 2000a, MNRAS, 315, 115
Dunne L., Clements D. L., Eales S., 2000b, MNRAS, 319, 813
Eales S. et al., 1999, ApJ, 515, 524

Eales S., Lilly S., Webb T., Dunne L., Gear W., Clements D., Yun M., 2000, AJ, 120, 2244
Efstathiou A., Rowan-Robinson M., Siebenmorgen R., 2000a, MNRAS, 313, 734
Efstathiou A. et al., 2000b, MNRAS, 319, 1169
Elbaz D., 1999b, in Hammer F., Thuan T. X., Cayette V., Guideroni B., Tran Thuan Van J., eds, Building the Galaxies from the Primordial Universe to the Arcs, XIX Moriand Astrophysics Meeting, March 1999. Editions Frontières, Gif-sur-Yvette (astro-ph/9911050)
Elbaz D., 2000, in Lemke D., Stickel M. K., eds, *ISO* Surveys of a Dusty Universe. Springer-Verlag, Tegernsee, p. 121
Elbaz D., Aussel H., Baker A. C., 1998, Proc. 34th Liege International Astrophysics Colloquium on the Next Generation Space Telescope. Univ. Liege, Belgium, p. 47
Elbaz D. et al., 1999, A&A, 351, L37
Ellis R., 1987, in Hewitt A., Burbidge G., Fang L.-Z., eds, Proc. IAU Symp. 124, Observational Cosmology. Reidel, Dordrecht, p. 367
Finkbeiner D. P., Davis M., Schlegel D. J., 2000 (astro-ph/0004175)
Fixsen D. J., Dwek E., Mather J. C., Bennet C. L., Shafer R. A., 1998, ApJ, 508, 123
Flores H. et al., 1999a, ApJ, 517, 148
Flores H. et al., 1999b, A&A, 343, 389
Franceschini A., Mazzei P., De Zotti G., Danese L., 1994, ApJ, 427, 140
Franceschini A. et al., 1998, ApJ, 506, 600
Frayer D. T., Ivison R. J., Scoville N. Z., 1998, ApJ, 506, L7
Frayer D. T., Ivison R. J., Scoville N. Z., 1999, ApJ, 514, L13
Gispert R., Lagache G., Puget J-L., 2000, A&A, 360, 1
Gregorich D. T., Neugebauer G., Soifer B. T., Gunn J. E., Herter T. L., 1995, AJ, 110, 259
Guiderdoni B., Hivon E., Bouchet F. R., Maffei B., 1997, in Bouchet F. R., Gispert R., Guiderdoni B., Tran Tranh Van J., eds, Proc. XVIth Moriond Astrophysics Meeting, Microwave Background Anisotropies. Editions Frontières, Gif-sur-Yvette, p. 419
Guiderdoni B., Hivon E., Bouchet F. R., Maffei B., 1998, MNRAS, 295, 877
Hacking P. B., Houck J. R., 1987, ApJS, 63, 311
Hassinger G., 1998, Astron. Nachr., 319, 37
Hauser M. G. et al., 1998, ApJ, 508, 25
Helou G., Soifer B. T., Rowan-Robinson M., 1984, BAAS, 16, 471
Holland W. et al., 1999, MNRAS, 303, 659
Hughes D. H., 2000a, in Mangum J. G., Radford S. J. E., eds, ASP Conf. Ser. Vol. 217, Imaging at Radio Through Submillimeter Wavelengths. Astron. Soc. Pac., San Francisco
Hughes D., 2000b, in Beckman J. E., Mahoney T. J., eds, ASP Conf. Ser., The Evolution of Galaxies on Cosmological Timescales. Astron. Soc. Pac., San Francisco, p. 11
Hughes D. et al., 1998, Nat, 457, 616
Kawada M., 1998, in Fowler A. M., ed., Proc. SPIE, 3354. p. 905
Kawara K. et al., 1998, A&A, 336, L9
Kawara K. et al., 2000, in Lemke D., Stickel M. K., eds, *ISO* Surveys of a Dusty Universe. Springer-Verlag, Tegernsee, p. 51
Kessler M. et al., 1996, A&A, 315, L27
Kim D. C., Sanders D. B., 1998, ApJS, 119, 41
Kirshner R. P., Oemler A., Jr, Schechter P. L., Shectman S. A., 1981, ApJ, 248, L57
Kormendy J., Sanders D. B., 1992, ApJ, 390, L53
Lagache G., Abergel A., Boulanger F., Desert F. X., Puget J-L., 1999, A&A, 344, 322
Lagache G., Haffner L. M., Reynolds R. J., Tufte S. L., 2000, A&A, 354, 247
Lawrence A., Walker D., Rowan-Robinson M., Leech K. J., Penston M. V., 1986, MNRAS, 219, 687
Lilly S. J., Le Fevre O., Hammer F., Crampton D. D., 1996, ApJ, 460, L1
Lilly S. J., Eales S. A., Gear W. K. P., Hammer F., Le Fevre O., Crompton D., Bond R. J., Dunne L., 1999, ApJ, 518, 641
Lindern-Vørnle M. J. D. et al., 2000, A&A, 359, L51
Lonsdale C. J., 1996, in Dwek E., ed., AIP Conf. Proc., Unveiling the Cosmic Infrared Background. AIP, New York, p. 348

Lonsdale C. J., Hacking P. B., Conrow T. P., Rowan-Robinson M., 1990, ApJ, 358, 60

Lu N. Y. et al., 1996, BAAS, 28, 1356

Lutz D. et al., 1997, A&AS, 248, 217

Madau P., Ferguson H. C., Dickenson M. E., Giavalisco M., Steidel C., Fruchter A., 1996, MNRAS, 283, 1388

Mann R. G. et al., 1997, MNRAS, 289, 482

Matsuhara H., 1998, in Fowler A. M., eds, Proc. SPIE, 3354, 915

Matsuhara H. et al., 2000, A&A, 361, 407

Matsumoto T. et al., 2000, in Lemke D., Stickel M. K., eds, *ISO* Surveys of a Dusty Universe. Springer-Verlag, p. 99

McClure R. J., Kukula M. J., Dunlop J. S., Baum S. A., O'Dea C. P., Hughes D. H., 1999, MNRAS, 308, 377

Melnick J., Mirabel I. F., 1990, A&A, 231, L9

Oliver S. J., Rowan-Robinson M., Saunders W., 1992, MNRAS, 256, 15P

Oliver S. J. et al., 1995, in Maddox S. J., Aragon-Salamanca A., eds, Wide Field Spectroscopy and the Distant Universe. World Scientific Press, Singapore, p. 274

Oliver S. J. et al., 1997, MNRAS, 289, 471

Oliver S. J. et al., 2000a, MNRAS, 316, 749

Oliver S. J. et al., 2000b, in Lemke D., Stickel M. K., eds, *ISO* Surveys of a Dusty Universe. Springer-Verlag, Tegernsee, p. 29

Ozernoy L., 2000, in Harwit M., Hauser M., eds, Proc. XXIVth IAU General Assembly, S204, The Extragalactic Infrared Background and its Cosmological Implications. Astron. Soc. Pac., San Francisco, p. 17

Peacock J. A. et al., 2000, MNRAS, 318, 535

Pearson C. P., Rowan-Robinson M., 1996, MNRAS, 283, 174 (cppRR)

Pearson C. P., Matsuhara H., Onaka T., Watarai H., Matsumoto T., 2001, MNRAS, 324, 999

Pilbrat G. L., 2000, in Lemke D., Stickel M. K., eds, *ISO* Surveys of a Dusty Universe. Springer-Verlag, Tegernsee, p. 408

Puget J. L., Leger A., 1989, ARA&A, 27, 161

Puget J. L., Abergel A., Bernard J.-P., Boulanger F., Burton W. B., Desert F.-X., Hartmann D., 1996, A&A, 308, L5

Puget J. L. et al., 1999, A&A, 345, 29

Rieke G. H., 2000, in Lemke D., Stickel M. K., eds, *ISO* Surveys of a Dusty Universe. Springer-Verlag, p. 403

Rowan-Robinson M., 1992, MNRAS, 258, 787

Rowan-Robinson M., 1995, MNRAS, 272, 737

Rowan-Robinson M., 2000, in Lemke D., Stickel M. K., eds, *ISO* Surveys of a Dusty Universe. Springer-Verlag, Tegernsee, p. 129

Rowan-Robinson M., Crawford P., 1989, MNRAS, 238, 523

Rowan-Robinson M., Efstathiou A., 1993, MNRAS, 263, 675

Rowan-Robinson M., Hughes J., Vedi K., Walker D. W., 1990, MNRAS, 246, 273

Rowan-Robinson M. et al., 1991a, Nat, 351, 719

Rowan-Robinson M. et al., 1991b, MNRAS, 253, 485

Rowan-Robinson M., Efsthiou A., Lawrence A., Oliver S., Taylor A., 1993, MNRAS, 261, 513

Rush B., Malkan M., Spinoglio L., 1993, ApJS, 89, 1

Sanders D. B., Soifer B. T., Elias J. H., Madore B. F., Matthews K., Neugebauer G., Scoville N. Z., 1998, ApJ, 325, 74

Saunders W., 1990, PhD thesis, Univ. London

Saunders W., Rowan-Robinson M., Lawrence A., Efstathiou G., Kaiser N., Ellis R. S., 1990, MNRAS, 242, 318

Schloerb F. P., 1997, Proc. IAU, 170, 221

Serjeant S. B. G. et al., 1997, MNRAS, 289, 457

Serjeant S. B. G. et al., 2000, MNRAS, 316, 768

Siebenmorgen R., Krugel E., 1992, A&A, 259, 614

Smail I., Ivison R. J., Blain A. W., 1997, ApJ, 490, L5

Smail I., Ivison R. J., Kneib J.-P., Cowie L. L., Blain A. W., Berger A. J., Owen F. N., Morrison G., 1999, MNRAS, 308, 1061

Smail I., Ivison R. J., Owen F. N., Blain A. W., Kneib J.-P., 2000, ApJ (astro-ph/9907083v3)

Soifer B. T., Sanders D. B., Madore B. F., Neugebauer G., Danielson G. E., Elias J. H., Lonsdale C. J., Rice W. L., 1987a, ApJ, 320, 238

Soucail G., Kneib J. P., Bezecourt J., Metcalfe L., Altieri B., Le Borgne J. F., 1999, A&A, 343, L70

Stecker F., 2000, in Harwit M., Hauser M., eds, Proc. XXIVth IAU General Assembly, S204 The Extragalactic Infrared Background and its Cosmological Implications. Astron. Soc. Pac., San Francisco, p. 135

Stickel M. et al., 1998, A&A, 336, 116

Surace J. A., Sanders D. B., Vacca W. D., Veilleux S., Mazzarella J. M., 1998, ApJ, 492, 116

Takahashi H. et al., 2000, in Breckinridge J. B., ed., Proc. SPIE, 4013, 47

Takeuchi T. T., Hirashita H., Ohta K., Hattori G. T., Ishii T. T., Shibai H., 1999, PASP, 111, 288

Takeuchi T. T., Ishii T., Hirashita H., Yoshikawa K., Matsuhara H., Kawara K., Okuda H., 2001, PASJ, 53, 37

Taniguchi Y. et al., 1997, A&A, 328, L9

Trentham N., 2000, MNRAS, 323, 542

Vigroux L. et al., 1996, A&A, 315, L93

Watarai H. et al., 2000, Breckinridge J. B., ed., Proc. SPIE, 4013, 59

Xu C. et al., 1998, ApJ, 508, 576

This paper has been typeset from a TEX/LATEX file prepared by the author.